INSTITUTIONAL LISTINGS

The IRE Professional Group on Microwave Theory and Techniques is grateful for the assistance given by the firms listed below, and invites application for Institutional Listing from other firms interested in the Microwave field.

CASCADE RESEARCH CORPORATION, 53 Victory Lane, Los Gatos, Calif.
Res., Dev., & Prod. Microwave Ferrite Devices, Backward Wave Oscillators & Microwave Test Equip.

COLLINS RADIO CO., Cedar Rapids, Iowa
Complete Industrial Microwave, Communication, Navigation and Flight Control Systems

HUGHES AIRCRAFT COMPANY, Culver City, California
Radar Systems, Guided Missiles, Antennas, Radomes, Tubes, Solid State Physics, Computers

MARYLAND ELECTRONIC MANUFACTURING CORPORATION, College Park, Md.
Development and Production of Microwave Antennas and Waveguide Components

(Please see back cover for additional listings.)

IRE Transactions

on Microwave Theory and Techniques

Volume MTT-5 **JANUARY, 1957** Number 1

In This Issue

For complete Table of Contents, see page 1.

PUBLISHED BY THE
Professional Group on Microwave Theory and Techniques

IRE Transactions on Microwave Theory and Techniques

Published by the Professional Group on Microwave Theory and Techniques

Volume MTT-5 JANUARY, 1957 Number 1

TABLE OF CONTENTS

J. R. Whinnery

John R. Whinnery was born on July 26, 1916 in Read, Colo. He received the B.S. degree in electrical engineering from the University of California in 1937, and immediately went to work for the General Electric Company in Schenectady, N. Y.

At the General Electric Company, Mr. Whinnery entered the three-year Advanced Engineering Program, and following that, supervised the high-frequency part of that program for two years. He then worked in the Electronics Laboratory and the Research Laboratory on problems in velocity-modulation tubes, traveling-wave tubes, and disk-seal triodes. In 1945–1946 he was also part-time lecturer in Union College.

In 1946, Mr. Whinnery returned to the University of California to teach electrical engineering and to complete work on his Ph.D. degree. He is now professor of electrical engineering there and chairman of the Electrical Engineering Division. During summer periods he has worked at Stanford University, the Hughes Aircraft Company, and the Ramo-Wooldridge Corporation, and during an industrial leave in 1951–1952 he was head of the Microwave Section of the Hughes Electron Tube Laboratory.

Mr. Whinnery is co-author with Simon Ramo of the text "Fields and Waves in Modern Radio," and is also author of several journal papers on waveguide discontinuities, antenna problems, and microwave tubes.

Mr. Whinnery became an associate member of the IRE in 1941, a senior member in 1944, and received the Fellow award in 1952. He held offices in the San Francisco Section from 1948 to 1954, becoming chairman in 1953, and has been active in WESCON and on many national IRE committees. He is now a director-at-large of the IRE.

The Next Problem in Engineering Education

JOHN R. WHINNERY
University of California, Berkeley, California

We have read very much in the past few years of the need for more engineers, so I shall not repeat the arguments here. Many of you have taken part in the very excellent programs designed to acquaint high school students with the opportunities in an engineering career, and I should first like to point out how successful these programs have been. This fact, I believe, is not generally realized. To use our own school as an example, enrollments during the past two years for the university as a whole have risen about 14 per cent, using the same standards of admitting only those among the upper 15 per cent of high school graduates. This rise reflects very nearly the increased birth rate at the end of the depression and the population growth of this area. During this same period, enrollment in engineering has increased about 50 per cent, and in electrical engineering 80 per cent. Although we do not break down the fields of interest further in the early undergraduate years, I believe the proportion of those interested in the microwave field is remaining nearly constant in spite of the competition from several newer fields.

Now that there is success in this first step of stimulating interest in engineering among new students, we must pass to the next one and ask, "What do we do with them?"

All who have thought about the problem know that we must be concerned with quality as much or more than quantity. If we start to measure our success by the number of engineering degrees compared with some carefully estimated quota, or with those from a competitor in the cold war, we are lost.

Our technology continues to become more complicated, and it is recognized that the quality and level of instruction must be improved. However, there exist many pressures toward downgrading, for as numbers of entrants increase, the difficulties of keeping a first-quality staff in the face of the fierce industrial competition also increase. This is of course not the fault of the industries, for they only recognize a real situation. Strictly speaking, it is up to the universities also to recognize it, even though it is difficult within the relatively inelastic educational budgets. The problem has been solved in a few schools, but I believe it is correct to say that in a majority of them, including many of the fine small ones, it is getting worse.

Both government and industry now help the universities in a very large way through sponsored research programs, fellowships, grants-in-aid, and cooperative programs. Many, in recognizing the seriousness of the problem, have felt that government and industry as a whole should do something more drastic, on a larger scale, and at once. If such emergency steps are taken, they must be taken with great wisdom so that the "shock wave" does not destroy the system it is planned to save. In any event the seriousness of the problem should be recognized and all possible solutions debated. We in schools will in the meantime need the continued support and advice from our friends in government and industry.

Broad-Band Balanced Duplexers*

CLARENCE W. JONES†

Summary—**Balanced duplexer circuits are described and a comparison is made between the two principal configurations employing gaseous switching devices. The balanced tr duplexer is limited in power-handling ability, while the balanced atr duplexer has slightly greater received-signal insertion loss. An analysis is made of the reflecting properties of an atr array, and the practical upper limit of the number of array elements is determined.**

A DUPLEXER, in the language of radar, is a switching device which disconnects the transmitter from the receiver, usually by means of gaseous discharge tubes called tr's and atr's. There are at least three principal types of duplexers, each of which may have several variations dependent upon the specific application, power level to be handled, or bandwidth required. These types are: 1) branching duplexer, 2) polarization-twist duplexer, and 3) balanced duplexer. This classification does not cover all of the possible configurations of duplexers which employ gaseous discharge switches, nor does it include the duplexers employing ferrite-switching elements, although a large percentage of these ferrite devices could be included under categories 2) and 3).

The bandwidth of a duplexer is determined by both the bandwidths of the switching tubes, tr's and atr's, and the circuit configuration. The branching duplexer is the simplest configuration but is not inherently broad band. Its performance near the band edges is greatly influenced by the transmitter impedance. Both the polarization-twist and the balanced-duplexer characteristics are unaffected by the transmitter impedance within the useful pass band. The balanced duplexer is inherently capable of the greatest bandwidth, in principle being limited only by the waveguide bandwidth.

Balanced duplexers can take on many physical shapes. They may be built in coaxial line with ring hybrids or quarter-wave coaxial hybrids,[1] in slab line using circuits equivalent to the coaxial circuits, or in waveguide with ring hybrids,[2] directional couplers, or magic tees.[2] The switching circuits may employ either narrow-band or broad-band tr and atr elements of waveguide or coaxial construction. It is also possible to mix the waveguide and coaxial construction if this has an advantage in a particular application.

* Original manuscript received by the PGMTT, April 2, 1956. The research in this document was supported jointly by the U. S. Army, Navy, and Air Force under contract with Mass. Inst. Tech., Cambridge, Mass.

† Lincoln Lab., M.I.T., Lexington, Mass.

[1] C. G. Montgomery, R. H. Dicke, and E. M. Purcell, M.I.T. Rad. Lab. Ser., McGraw-Hill Book Co., Inc., New York, N. Y., vol. 8, ch. 12, 1948.

[2] L. D. Smullin and C. G. Montgomery, "Microwave Duplexers," M.I.T. Rad. Lab. Ser., McGraw-Hill Book Co., Inc., New York, N. Y., vol. 14, ch. 8, 1948.

It is the purpose of this paper to analyze the operation of balanced duplexers, in particular the configurations employing directional coupler hybrid junctions. The analysis is best carried out through use of the scattering matrix.

Scattering Matrix Representation of Microwave Circuits

The scattering matrix representation[3] lends itself admirably to a large number of microwave problems, and will be used here in so far as practical to describe the behavior of balanced duplexers. The scattering matrix relates the waves traveling outward at a set of n terminals to those waves traveling inward at the set of terminals. S will be used to designate a scattering matrix, with subscripts added where appropriate in order to avoid confusion. Thus we may write

$$\begin{bmatrix} E_{01} \\ E_{02} \\ \vdots \\ E_{0n} \end{bmatrix} = \begin{bmatrix} S_{11} & S_{12} \cdots S_{1n} \\ \cdots\cdots\cdots \\ S_{n1} \cdots\cdots S_{nn} \end{bmatrix} \begin{bmatrix} E_{i1} \\ E_{i2} \\ \vdots \\ E_{in} \end{bmatrix}. \tag{1}$$

The terms on the major diagonal, S_{11}, S_{22}, $\cdots$, etc., are the reflection coefficients that would be measured if all other terminals were terminated with a match. All other matrix elements are transfer terms, again applying to the case where the terminals are reflectionless.

In order to solve the duplexer problem represented by Fig. 1, it is necessary to obtain the scattering matrices for the switching elements and the hybrids. The switching element is a two-terminal device and can be represented by

$$S_s = \begin{bmatrix} S_{11} & S_{12} \\ S_{12} & S_{11} \end{bmatrix}. \tag{2}$$

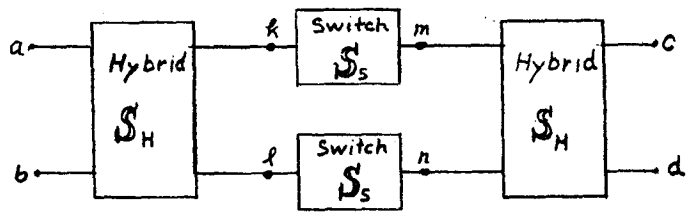

Fig. 1—Balanced duplexer.

The matrix is completely symmetrical because the reflection and transfer characteristics are the same when viewed from either terminal. The switch is a passive bi-

[3] Montgomery, Dicke, and Purcell, *op. cit.*, ch. 5.

lateral device which has two operating conditions. S_{11} and S_{12} have two sets of values, one during the time the transmitter is on, and the other during the time the radar is receiving. More will be said about this in a later section.

The hybrid is a four-terminal device which ideally has the property that power supplied to a given terminal is equally divided between two of the three remaining terminals and nothing is coupled to the fourth terminal. It is possible to build hybrids which have a high degree of isolation and acceptable balance over a very wide band. For example, a multiple slot hybrid can have a directivity of 40 db and a deviation from 3 db coupling of 0.3 db over the 40 per cent waveguide band. If one properly numbers the terminals, the scattering matrix for an ideal directional coupler hybrid may be written

$$S_H = \frac{1}{\sqrt{2}}\left[\begin{array}{cc|cc} 0 & 0 & 1 & j \\ 0 & 0 & j & 1 \\ \hline 1 & j & 0 & 0 \\ j & 1 & 0 & 0 \end{array}\right]. \tag{3}$$

The term S_{12} is zero by definition for a perfect hybrid and so small in a practical unit that it can be set equal to zero without appreciable error. It can be proved[4] that for $S_{12}=0$, $S_{11}=0$ also. In general the hybrids cannot be considered perfect, but for the case of the directional coupler hybrid, of either the multi-slot or the short-slot type, it has been found that calculations are sufficiently accurate if it is assumed that only the power split departs from ideal. The scattering matrix for this case may be written

$$S_H = \left[\begin{array}{c|c} 0 & H \\ \hline H & 0 \end{array}\right], \tag{4}$$

where H is a submatrix which contains the terms describing the power split. Eq. (4) applies to all types of hybrid circuits whose isolation is sufficiently good that S_{12} may be neglected. The form of H is different for directional coupler hybrids than for magic tee and ring hybrids and, as a result, the circuit configurations vary with the type of hybrid or combinations of hybrids used. Fig. 2 illustrates this. The scattering matrix for ideal ring hybrids or magic tees (5) may be compared to the scattering matrix for the ideal directional-coupler hybrid (3).

$$S_T = \frac{1}{\sqrt{2}}\left[\begin{array}{cc|cc} 0 & 0 & 1 & 1 \\ 0 & 0 & -1 & 1 \\ \hline 1 & -1 & 0 & 0 \\ 1 & 1 & 0 & 0 \end{array}\right]. \tag{5}$$

The directional-coupler hybrid provides the duplexer circuit with the highest degree of symmetry, which would lead one to believe that this configuration should be capable of the greatest bandwidth. For purposes of this paper, only this type of duplexer will be considered from this point on.

[4] *Ibid.*, ch. 9.

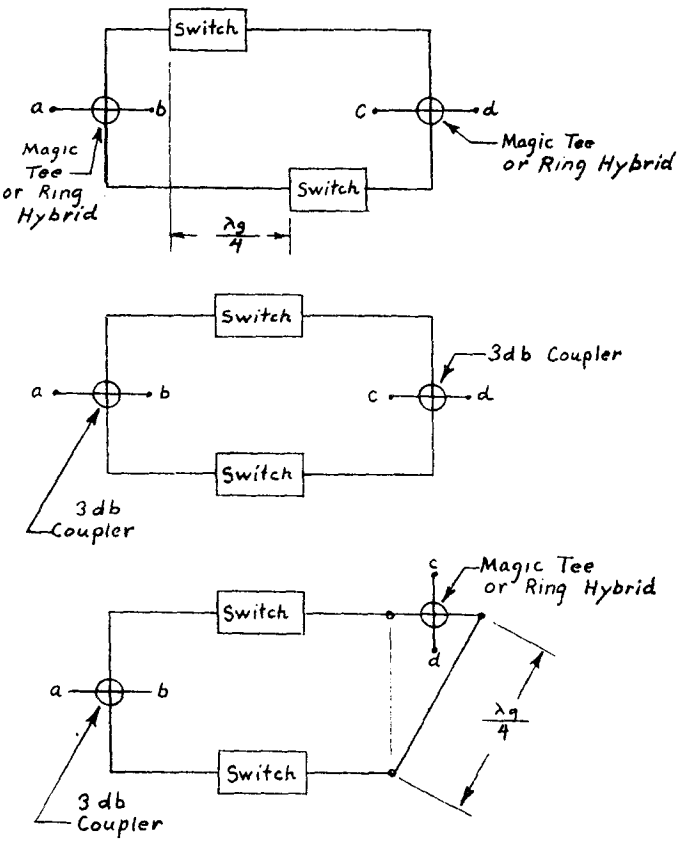

Fig. 2—Several possible balanced-duplexer configurations.

Balanced Hybrid Duplexer Theory

Scattering Matrix of the Duplexer

Using nomenclature of Fig. 1, rearranging the scattering equations for identical switches, one can write

$$\begin{bmatrix} E_{0k} \\ E_{0l} \end{bmatrix} = S_{11}\begin{bmatrix} E_{ik} \\ E_{il} \end{bmatrix} + S_{12}\begin{bmatrix} E_{im} \\ E_{in} \end{bmatrix}. \tag{6}$$

The matrix equation for the duplexer then becomes

$$\begin{bmatrix} E_{0a} \\ E_{0b} \\ E_{0c} \\ E_{0d} \end{bmatrix} = \left[\begin{array}{cc|cc} S_{11} & H^2 & S_{12} & H^2 \\ \hline S_{12} & H^2 & S_{11} & H^2 \end{array}\right]\begin{bmatrix} E_{ia} \\ E_{ib} \\ E_{ic} \\ E_{id} \end{bmatrix}. \tag{7}$$

H is the submatrix of (4) and may be written

$$H = \begin{bmatrix} \sqrt{\frac{1+\alpha}{2}} & j\sqrt{\frac{1-\alpha}{2}} \\ j\sqrt{\frac{1-\alpha}{2}} & \sqrt{\frac{1+\alpha}{2}} \end{bmatrix}, \tag{8}$$

where α is a frequency-sensitive term governing the power split. Values of α by definition must lie in the range $-1 \leqq \alpha \leqq 1$.

There are two principal types of balanced duplexers. The first employs balanced tr switches which reflect the transmitted power into the antenna. The second type employs balanced arrays of atr tubes which reflect the received signal into the receiver. These will be designated type I and type II respectively. The principal pieces of information desired are the relationships between the transmitter and antenna during the transmitting period and between the receiver and antenna during the receiving period. To determine this, it is necessary to reduce (7) to one involving only two of the four terminals. This can be done by terminating each of the other two terminals with a load having a reflection coefficient Γ. The two cases of interest are where 1) two terminals at the same end of the duplexer such as a and b of Fig. 1 are to be related, and 2) diagonally opposite terminals such as a and d are to be related.

After rearranging (7) and introducing the reflection coefficients Γ_c and Γ_d at the corresponding terminals, one may write the matrix equation

$$\begin{bmatrix} E_{0a} \\ E_{0b} \end{bmatrix} = \left(S_{11}P + S_{12}^2 \sum_{n=1}^{\infty} S_{11}^{n-1}(P\Gamma_1)^n P \right) \begin{bmatrix} E_{ia} \\ E_{ib} \end{bmatrix}, \quad (9)$$

where

$$P = H^2 = \begin{bmatrix} \alpha & j\sqrt{1-\alpha^2} \\ j\sqrt{1-\alpha^2} & \alpha \end{bmatrix} \quad (10)$$

$$\Gamma_1 = \begin{bmatrix} \Gamma_c & 0 \\ 0 & \Gamma_d \end{bmatrix}. \quad (11)$$

Relating a to d with b and c terminated gives

$$\begin{bmatrix} E_{0a} \\ E_{0d} \end{bmatrix} = \left(A + B \sum_{n=1}^{\infty} (\Gamma_2 A)^{n-1} \Gamma_2 B \right) \begin{bmatrix} E_{ia} \\ E_{ib} \end{bmatrix} \quad (12)$$

where

$$A = \begin{bmatrix} S_{11}P_{11} & S_{12}P_{12} \\ S_{12}P_{12} & S_{11}P_{11} \end{bmatrix} \quad (13)$$

$$B = \begin{bmatrix} S_{11}P_{12} & S_{12}P_{11} \\ S_{12}P_{11} & S_{11}P_{12} \end{bmatrix} \quad (14)$$

$$\Gamma_2 = \begin{bmatrix} \Gamma_b & 0 \\ 0 & \Gamma_c \end{bmatrix}. \quad (15)$$

Eqs. (9) and (12) describe the circuit characteristics of the two types of balanced duplexers being considered here. From them can be computed the vswr and insertion loss during both the transmitting and receiving phases. This is done by supplying the appropriate values of S_{11} and S_{12}, the switch tube parameters, which assume widely different values for the two operating conditions.

The Transmitting Condition

While the radar is transmitting, the tr and atr tubes will be ionized and may be represented by a short circuit. There is a finite voltage across these switches, but this is, in any practical case, several orders of magnitude below the line voltage and may be ignored.

In the case of the type I duplexer the tr tubes place a short circuit across the transmission line so that $S_{11} = -1$ and $S_{12} = 0$. Substituting this into (9) gives

$$\begin{bmatrix} E_{0a} \\ E_{0b} \end{bmatrix} = -1 \begin{bmatrix} \alpha & j\sqrt{1-\alpha^2} \\ j\sqrt{1-\alpha^2} & \alpha \end{bmatrix} \begin{bmatrix} E_{ia} \\ E_{ib} \end{bmatrix}. \quad (16)$$

The vswr seen by the transmitter is

$$R_{T1} = \frac{1+\alpha}{1-\alpha} \quad (17)$$

and the insertion loss (neglecting the loss in the gas discharge) expressed in db is

$$L_{T1} = 10 \log \frac{1}{1-\alpha^2}. \quad (18)$$

For the type II duplexer where the atr windows are in the plane of the waveguide walls, the application of high power produces a discharge which shorts out these windows and the switch section appears like a piece of unperturbed transmission line except for the negligible voltage across the window. For this case $S_{11} = 0$ and $S_{12} = 1$. Substituting into (12) and expanding to $n = 1$

$$\begin{bmatrix} E_{0a} \\ E_{0b} \end{bmatrix} = \begin{bmatrix} \Gamma_c\alpha^2 & j\sqrt{1-\alpha^2} \\ j\sqrt{1-\alpha^2} & \Gamma_b\alpha^2 \end{bmatrix} \begin{bmatrix} E_{ia} \\ E_{ib} \end{bmatrix}. \quad (19)$$

Terms of order higher than $n = 1$ will be multiplied by the factor $\Gamma_b\Gamma_c$. Γ_b is arbitrary and is usually made to equal zero by connecting a matched load to terminal b. Terminal c is connected to the receiver, which will normally be protected by an auxiliary tr tube. This will provide a short circuit at terminal c so we may set $\Gamma_c = 1$.

The vswr becomes

$$R_{T2} = \frac{1+\alpha^2}{1-\alpha^2}. \quad (20)$$

The insertion loss is the same as for the type I duplexer. In this case the reflected power is absorbed in the termination at terminal b rather than being reflected back into the transmitter.

The dissipation in the switch tubes is not considered in (18) and is obviously so small as to have negligible effect on the circuit performance as seen at the terminals. However in a high power radar the switch tube dissipation is very important, since it is one of the principal power limiting factors. While it is not possible to calculate accurately the switch tube dissipation, it is possible to make a comparison between the power-handling capabilities of the two duplexer systems if it is assumed that the switch tube windows are identical. This is not an unrealistic situation and affords a good starting point when considering power handling capabilities.

At the output of the first hybrid the currents will be $1/\sqrt{2}I_0$, assuming perfect hybrid balance, where I_0 is the line current at the input terminal corresponding to a power P_0. For the case of the type I duplexer, the tr tubes present a short circuit at which the current doubles. The window current is therefore $\sqrt{2}I_0$. If I_0 is the maximum current which the window can handle, then it is readily calculated that the line power must be reduced to $\frac{1}{2}P_0$. For the type II duplexer, the atr windows will be required to handle only $1/\sqrt{2}I_0$ and it is therefore possible to raise the transmitter power to $2P_0$ before the window capabilities are exceeded. All other things being equal, one would expect the atr type duplexer to handle four times the average power which can be switched by the tr type duplexer.

The transmitter load impedance is of importance in many applications. A comparison of (17) and (20), which are plotted in Fig. 3, shows that for the case of imperfect hybrids the atr duplexer has considerable advantage over the type I.

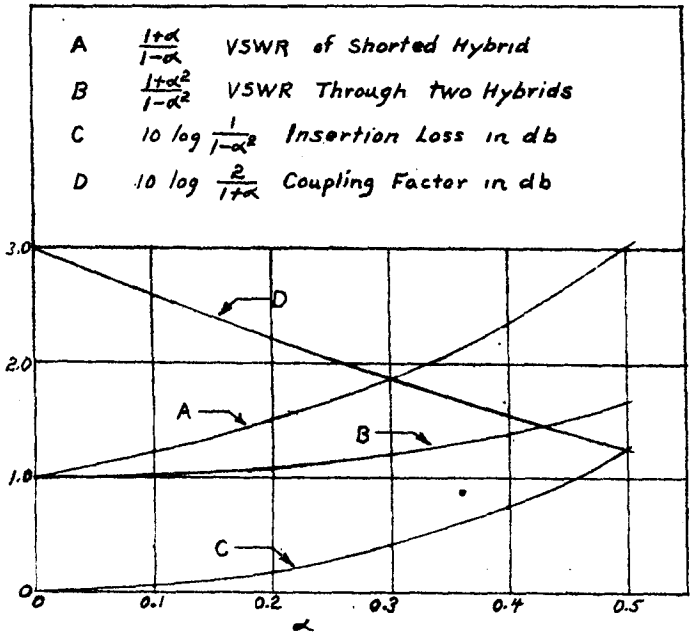

Fig. 3

The Receiving Condition

During the receiving interval, only very weak signals enter the duplexer, so the insertion loss between the antenna and receiver is the only feature of interest. The receiving situation with the type I duplexer is described by (12), where terminals a and d are the antenna and receiver respectively. Γ_b is the reflection coefficient of the transmitter, and Γ_c that of the arbitrary load. The insertion loss expanded to $n=1$ is

$$L_{R1}=20\log\left|\frac{1}{S_{12}\sqrt{1-\alpha^2}+S_{11}S_{12}\alpha\sqrt{1-\alpha^2}(\Gamma_b+\Gamma_c)}\right|. \quad (21)$$

Both S_{11} and α are normally small compared to unity within the useful pass band, so the second term in the denominator would ordinarily be neglected. S_{11} and S_{12} are the scattering coefficients for a particular tr switch.

The multiple-element broad-band tr tube is the switching element most used in the type I duplexer. This tube consists of several (usually two or three) quarter-wave-coupled resonant elements plus a low-Q window at each end which is also quarter-wave coupled to the other elements. There are a number of places in the literature where this type of band-pass filter is discussed.[6-7] Fig. 4 shows the band-pass characteristic for a 1B58, from which values of S_{11} and S_{12} can be estimated.

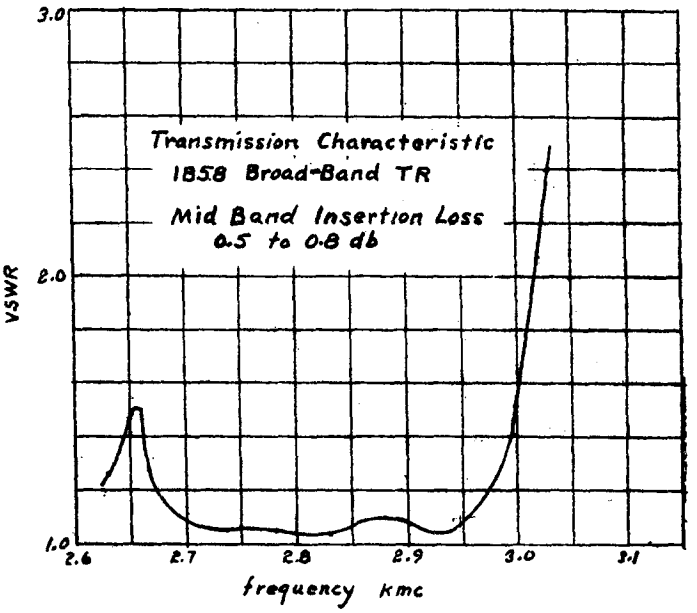

Fig. 4

During the receiving interval, the performance of the type II duplexer is described by (9). The switching circuit in this case is an array of one or more atr tubes. With the antenna at terminal a, the receiver at b, the transmitter having a reflection coefficient Γ_d at terminal d, and an arbitrary load of Γ_c at terminal c, the insertion loss expanded to $n=1$ is

$$L_{R2}=20\log\left|\frac{1}{S_{11}\sqrt{1-\alpha^2}+S_{12}^2\alpha\sqrt{1-\alpha^2}(\Gamma_c+\Gamma_d)}\right|. \quad (22)$$

In this case S_{11} and S_{12} are the scattering terms for an atr array.

With the exception of those instances where one is interested in the duplexer behavior outside of the pass

[5] W. L. Prichard, "Quarter wave coupled wave guide filters," *J. Appl. Phys.*, vol. 18, pp. 862–872; October, 1947.
[6] G. L. Ragan, "Microwave Transmission Circuits," M.I.T. Rad. Lab. Ser., McGraw-Hill Book Co., Inc., New York, N. Y., vol. 9, p. 683, 1948.
[7] Smullin and Montgomery, *op. cit.*, ch. 3.

band, the higher-order terms in the denominators of (21) and (22) can be ignored. In order to compare the performance of the two duplexers when receiving it is necessary to know the contributions to insertion loss made by the hybrids, the broad-band tr tubes, and the atr tube array. For type I

$$L_{R1} = 20 \log \left| \frac{1}{S_{12}} \right| + 20 \log \frac{1}{\sqrt{1 - \alpha^2}}, \tag{23}$$

where S_{12} is the transmission characteristic of the broad-band tr and α the balance factor of the hybrid. For type II, recalling that a broad-band tr is used in front of the receiver,

$$L_{R2} = 20 \log \left| \frac{1}{S_{11}} \right| + 20 \log \frac{1}{\sqrt{1 - \alpha^2}} + 20 \log \left| \frac{1}{S_{12}} \right|, \tag{24}$$

where S_{11} is the reflection factor of the atr tube array and S_{12} the transmission factor of the tr tube. All other things being equal it can be seen that the insertion loss of the atr duplexer is greater by the amount 20 log $|1/S_{11}|$.

The ATR Array

An atr tube is a shunt resonant circuit which is customarily mounted in series with the transmission line. An atr mounted on the broad surface of a rectangular waveguide is series mounted. When mounted on the narrow wall, the equivalent representation is a shunt circuit. The admittance matrix of the atr equivalent circuit, Fig. 5, is

$$Y = \begin{bmatrix} y & -y \\ -y & y \end{bmatrix} \tag{25}$$

where[8]

$$y = g + j2(1 + g)Q_L \frac{\Delta\omega}{\omega_0}. \tag{26}$$

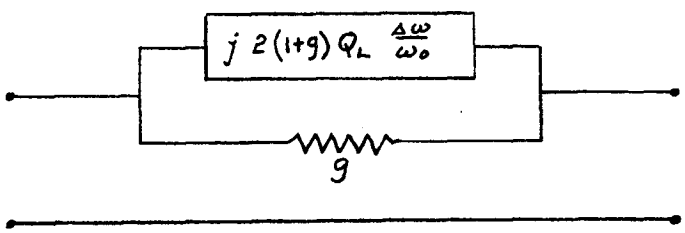

Fig. 5—Equivalent circuit of atr.

In order to compute the insertion loss of (22) it is necessary to obtain the scattering matrix for an array of tubes. This may be done by first obtaining the scattering matrix for a single tube using the relation[9]

$$S = (1 - Y)(1 + Y)^{-1} \tag{27}$$

with the result that

$$_1S = \frac{1}{1 + 2y} \begin{bmatrix} 1 & 2y \\ 2y & 1 \end{bmatrix}. \tag{28}$$

The second step is to cascade a line length θ with the atr circuit as shown in Fig. 6. This transformation[10] results in

$$S_\theta = \begin{bmatrix} S_{11} & S_{12}e^{-j\theta} \\ S_{12}e^{-j\theta} & S_{11}e^{-j2\theta} \end{bmatrix}. \tag{29}$$

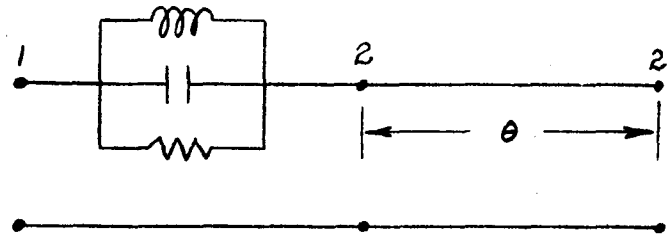

Fig. 6—Basic element of a tr array.

Except for the case where a line length is added at a terminal (29), the scattering matrix does not readily lend itself to cascading circuit elements. It is much more convenient at this point to transform to the T matrix[11,12] which has the form

$$\begin{bmatrix} E_{02} \\ E_{i2} \end{bmatrix} = T \begin{bmatrix} E_{i1} \\ E_{01} \end{bmatrix}. \tag{30}$$

To cascade n elements it is only necessary to multiply the T matrices in reverse order

$$_nT = T_nT_{n-1} \cdots T_1. \tag{31}$$

The transformations from the scattering matrix to the T matrix are

$$T = \begin{bmatrix} \left(S_{21} - \dfrac{S_{11}S_{22}}{S_{12}}\right) & \dfrac{S_{22}}{S_{12}} \\ -\dfrac{S_{11}}{S_{12}} & \dfrac{1}{S_{12}} \end{bmatrix} \tag{32a}$$

$$S = \begin{bmatrix} -\dfrac{T_{21}}{T_{22}} & \dfrac{1}{T_{22}} \\ \left(T_{11} - \dfrac{T_{12}T_{21}}{T_{22}}\right) & \dfrac{T_{12}}{T_{22}} \end{bmatrix}. \tag{32b}$$

The values of S_{11} for several arrays of identical atr tubes have been determined and are tabulated below.

[8] Smullin and Montgomery, *op. cit.*, p. 118.

[9] Montgomery, Dicke, and Purcell, *op. cit.*, p. 148.

[10] Montgomery, Dicke, and Purcell, *op. cit.*, p. 149.

[11] M. Tinkham and M. W. P. Strandberg, "The excitation of circular polarization in microwave cavities," Proc. IRE, *vol. 43*, pp. 734–738; June, 1955.

[12] Montgomery, Dicke, and Purcell, *op. cit.*, p. 150.

$$ {}_1S_{11} = \frac{1}{1+2y} \tag{33a}$$

$$ {}_2S_{11} = \frac{\frac{1-4y^2}{1+2y} - (1+2y)e^{j2\theta}}{1-(1+2y)^2e^{j2\theta}} \tag{33b}$$

$$ {}_3S_{11} = \frac{\frac{1-4y^2}{(1+2y)^2}[(1-4y^2)e^{-j2\theta} - (1+2y)^2] - [1-(1+2y)^2e^{j2\theta}]}{\frac{1}{1+2y}[(1-4y^2)e^{-j2\theta} - (1+2y)^2] - (1+2y)[1-(1+2y)^2e^{j2\theta}]} \tag{33c}$$

$$ {}_4S_{11} = \frac{\frac{1-4y^2}{(1+2y)^3}[(1-4y^2)^2e^{-j2\theta} - (3-4y^2)(1+2y)^2] + (1+2y)[3e^{j2\theta} - (1+2y)^2e^{j4\theta}] - 4y^2(1+2y)e^{j2\theta}}{\frac{1}{(1+2y)^2}[(1-4y^2)^2e^{-j2\theta} - (3-4y^2)(1+2y)^2] + (1+2y)^2[3e^{j2\theta} - (1+2y)^2e^{j4\theta}] + 4y^2} \tag{33d}$$

$$ {}_5S_{11} = \frac{\frac{1-4y^2}{(1+2y)^4}A - (1+2y)^2B - 4y^2[(3-4y^2)e^{j2\theta} - (1+2y)^2e^{j4\theta}]}{\frac{1}{(1+2y)^3}A - (1+2y)^3B + 4y^2\frac{1-4y^2}{1+2y}} \tag{33e}$$

where

$$A = (1-4y^2)^3e^{-j2\theta} - 4(1+2y)^2(1-4y^2)(1-j^2)$$

$$B = 6\frac{1-2y^2}{(1+2y)^2}e^{j2\theta} + 4e^{j4\theta} - (1+2y)^2e^{j6\theta}.$$

Fig. 7 (next page) consists of several plots of 20 log $1/S_{11}$. It can be demonstrated that half-wave spacing of identical atr tubes gives the widest pass band. Spacings different from half wave produce narrower pass bands or create "holes." Fig. 7(c), 7(d), 7(e), and 7(f) illustrates the effects of spacings different from half wave and indicate the spacing tolerance that must be held in order to maintain an acceptable pass band. An investigation of the effects of tuning errors in the atr circuits has not been attempted.

The curves of Fig. 7 have been plotted assuming an atr conductance of $g=0.02$. Several S-band tubes have been checked and it has been found that this is a realistic maximum figure. The resulting loss at band center is quite low, being less than 0.4 db for a single tube and less than 0.2 db for a three-tube array.

The 1-db insertion loss point has been arbitrarily chosen for bandwidth determination. The curve of Fig. 8 may be used for estimating bandwidth. This curve is a graphical determination from the data of Fig. 7 of the product BQ_L. It can be demonstrated that this product is very nearly constant for values of Q_L between three and ten. No attempt was made to obtain an explicit expression for $B=f(Q_L)$ because of the mathematical complexity. Fig. 8 shows that there is nothing to be gained by constructing arrays of more than four elements. In practice it may develop that a three-element array is the largest practicable because of tuning tolerances and other circuit features which have not been taken into account in this treatment.

Hybrid Characteristics

The short-slot hybrid[13] is extensively used in balanced duplexer applications. Where balanced tr tubes are used the hybrid is customarily the side wall type, in which case the coupling is accomplished by means of an aperture in the common narrow wall of the waveguide. The top wall coupler which has two slots in the common broad dimension of the waveguide can also be used, and is a convenient configuration of the atr duplexer. Of the two types of short-slot hybrids, the top wall configuration has the best pass-band characteristic, but the side wall coupler will handle the most power. An attempt has been made by H. J. Riblet, originator of these types of hybrids, to increase the power handling ability of the top wall coupler by increasing the radii on the common wall. This has met with some success, but sufficient data are not available to make a valid comparison of the two types. Fig. 9 is a photograph of these two hybrid junctions. Fig. 10 (p. 12), shows values of α measured for a single model each of the side wall coupler and low-power

[13] H. J. Riblet, "The short slot hybrid junction." Proc. IRE, vol. 40, pp. 180–184; February, 1952.

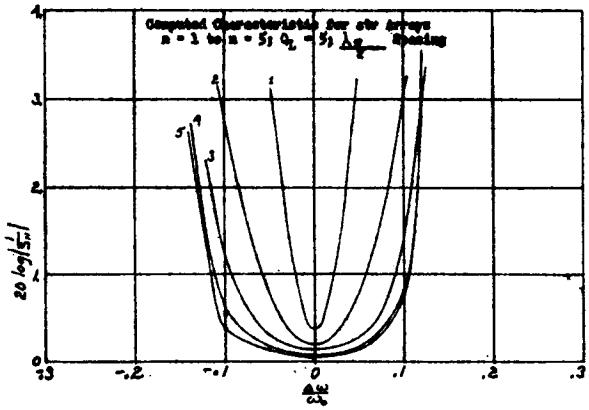

(a)

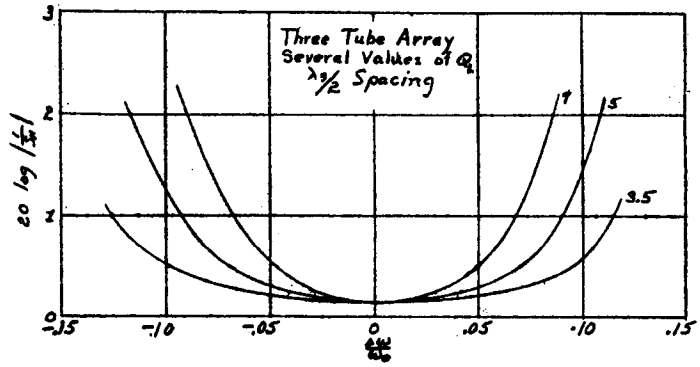

(b)

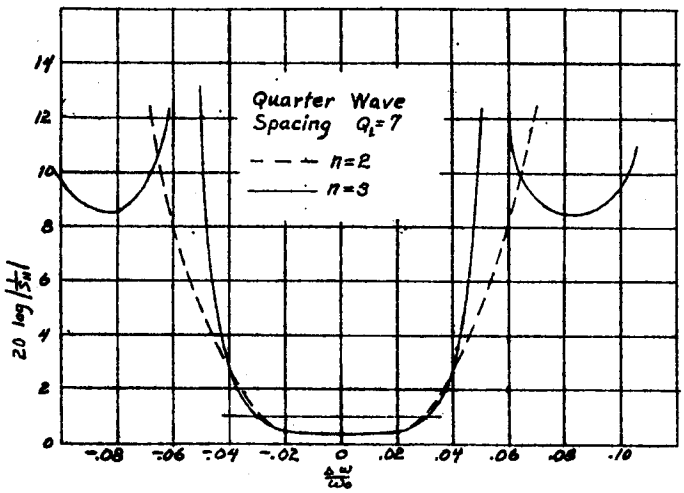

(c)

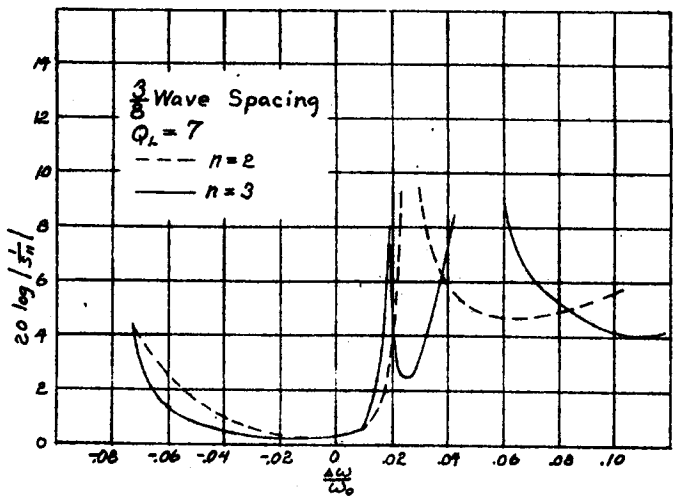

(d)

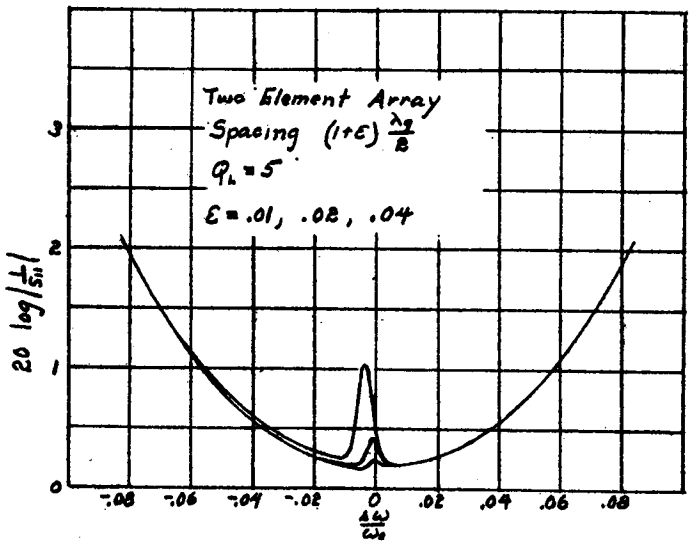

(e)

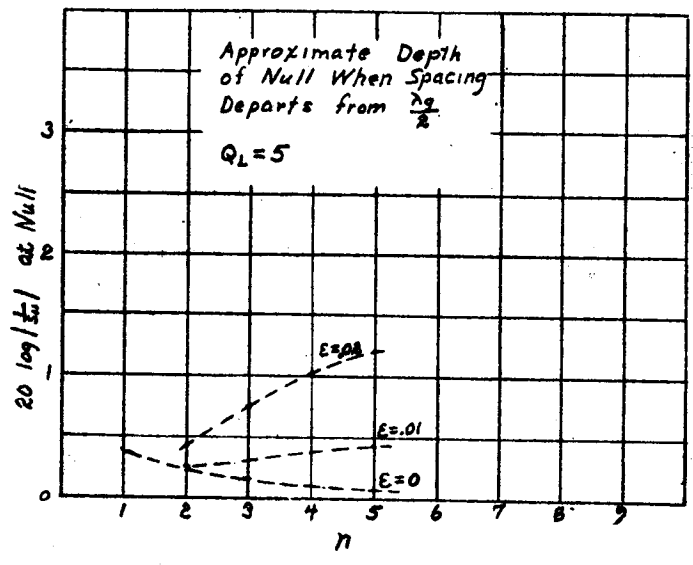

(f)

Fig. 7

top wall coupler, and the average of four models of the high power top wall coupler. In the latter case the units showed very little spread in characteristic over the band, 2600–3100 mc.

ATR Tubes

The choice of an atr tube array for the type II duplexer will be a compromise between bandwidth per

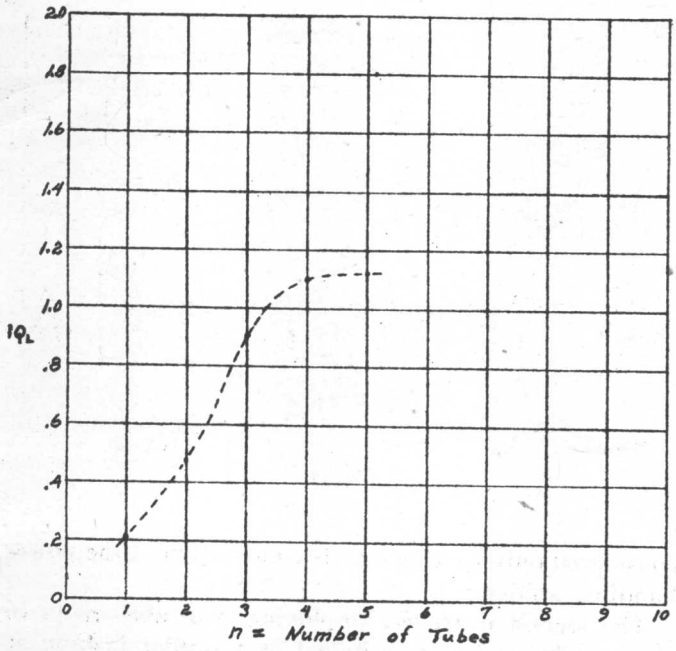

Fig. 8—Relationship between bandwidth ($B=\Delta\omega/\omega_0$ at 1 db) and number of half-wave spaced atr tubes.

Several *S*-band tubes have been procured from Bomac and Sylvania. Table I gives their low-level characteristics.

TABLE I*

Type	Q_L	mfr.
1B56	3.4	Bomac
1B56	3.3	Sylvania
BL623	5.5	Bomac
ATR788	5.5	Sylvania
BL632	9.4	Bomac

* $g \leqq 0.02$ for all tubes.

Experimental *S*-Band ATR Duplexer

Two atr duplexers were constructed, tested at low level, and then operated in radar systems in order to compare their performance with other existing duplexers. Unfortunately, the radars available did not have the transmitter power capabilities necessary for determining the useful upper limit of this type of duplexer. Some observations were made, however, which indicate that it is capable of handling high average power.

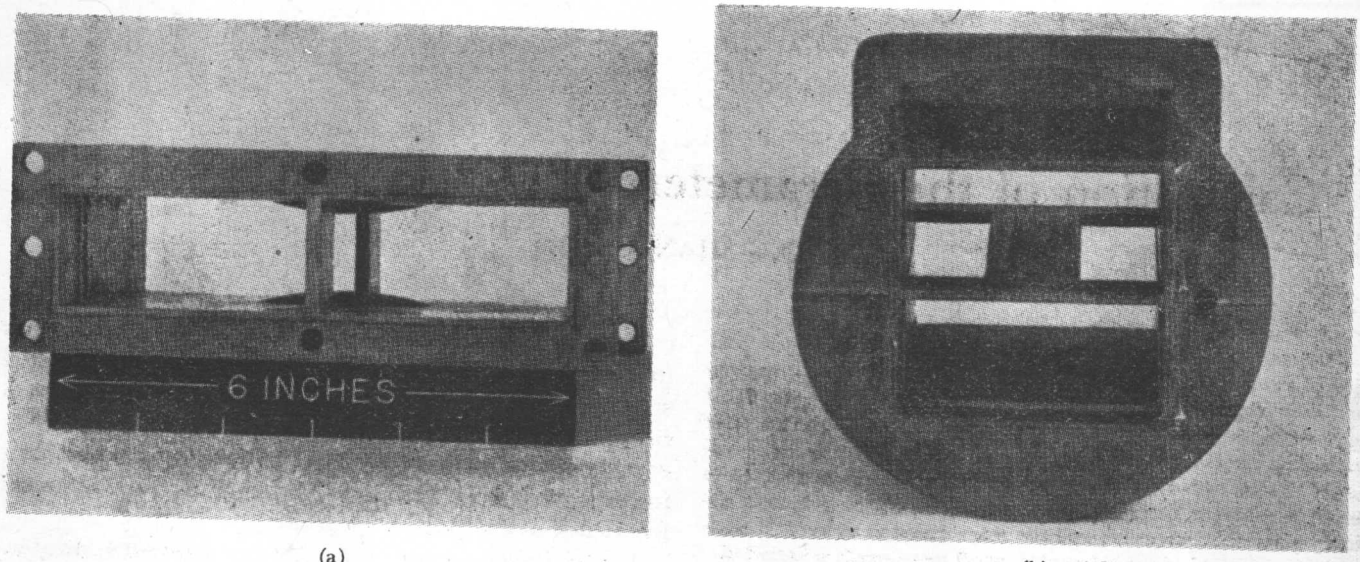

(a) (b)

Fig. 9

tube and high level dissipation per tube. The higher the Q_L the greater the number of tubes required for a given bandwidth, but since the high-Q tubes have narrow windows, the arc voltage should be lower and one might expect the power lost per tube to be reduced. Sufficient data are not yet available regarding the relationship between dissipation and Q_L to form any conclusions at this point, but observations seem to confirm the suspicion that the dissipation goes at least as rapidly as $1/Q_L$ in the range $Q_L=3.4$ to $Q_L=9.4$.

The first of these duplexers employed two BL623 atr tubes (single-tube array) as the switching elements. The receiving bandwidth, which was that of the atr array, was 3.6 per cent. Bandwidth is arbitrarily defined as the per cent frequency between 1-db points of the atr array characteristic, *i.e.*, $L=20\log\left|1/S_{11}\right|=1$. At 1.2 kw average power the switch tube temperature was about 140°F, as compared to a temperature in excess of 212°F for a 1B56 in a branching duplexer at the same power level. This is a crude comparison and should be

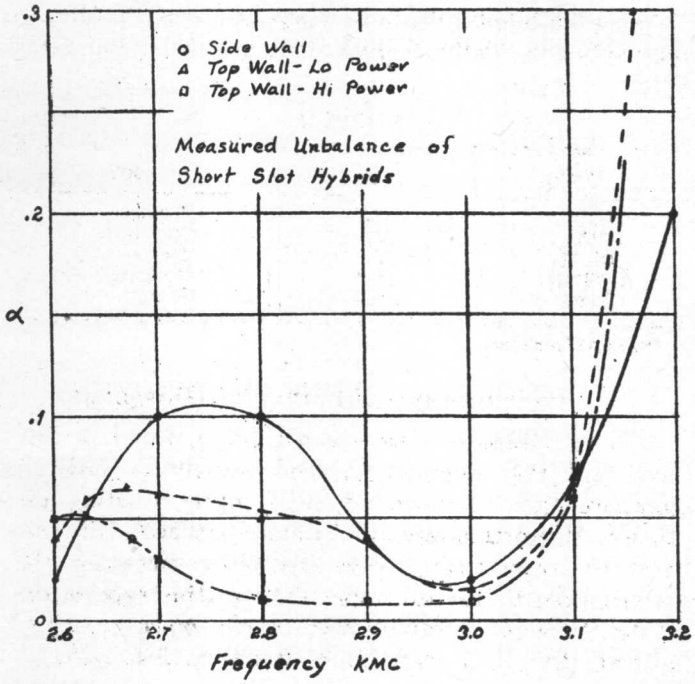

Fig. 10

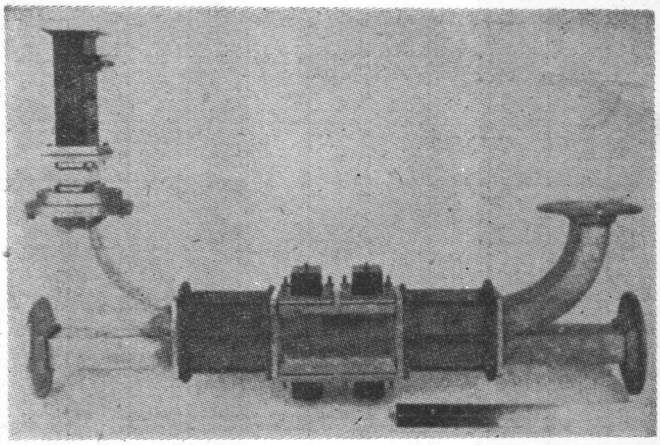

Fig. 11

considered only as a qualitative indication of the power handling ability.

The second duplexer, employing two-tube arrays in the switching circuit, behaved in a similar fashion at high level and had the predicted receiving bandwidth. This duplexer is shown in Fig. 11 (above).

Calculation of the Parameters of Ridge Waveguides*

TSUNG-SHAN CHEN†

Summary—**In this paper an algebraic expression which constitutes an approximation to Cohn's transcendental equation is given for the determination of the dominant-mode cutoff wavelength of ridge waveguides. A modified derivation of Mihran's equation for calculating the characteristic impedance of ridge waveguides is discussed. Based upon these formulas, nomographs are constructed to permit the determination of these parameters with sufficient accuracy when the waveguide and the ridge dimensions vary. Experimental verification of the calculated cutoff wavelength is included.**

Introduction

RIDGE WAVEGUIDES have a longer cutoff wavelength and a lower characteristic impedance than conventional rectangular waveguides having the same internal dimensions. The ridge waveguides also have a wider bandwidth free from higher-mode interference. Because of these advantages, ridge waveguides have been used as transmission links in systems requiring a wide free range in the fundamental mode,[1] as matching or transition elements in waveguide-to-coaxial junctions,[2] as filter elements, and as components for other special purposes.[3] One type of slow-wave structure used with traveling-wave tubes consists of a ridge waveguide which is made periodic by means of equally spaced transverse slots. The transverse resonant frequency of this structure corresponds to the cutoff frequency of the ridge waveguide.[4]

In the development of tunable magnetrons, double-ridge waveguides have been used as external tuning cavities because their reduced cutoff frequency permits a compact cavity section. Because the electric field is concentrated between the ridges, satisfactory tuning characteristics are obtained by means of a plunger which short-circuits the narrow gap. In the electron-beam method of frequency modulation, the beam is introduced in this region of strong electric field between two parallel plates attached to the ridges.

* Manuscript received by PGMTT, March 14, 1956.
† Radio Corp. of America, Harrison, N. J.

[1] T. N. Anderson, "Double-ridge waveguide for commercial airlines weather radar installation," IRE TRANS., vol. MTT-3, pp. 2–9; July, 1955.

[2] Radio Res. Lab. Staff, Harvard Univ., "Very High-Frequency Techniques," vol. II, pp. 678–684, 731–736, McGraw-Hill Book Co., Inc., New York, N. Y.; 1947.

[3] S. B. Cohn, "Properties of ridge waveguides," PROC. IRE, vol. 35, pp. 783–788; August, 1947.

[4] J. R. Pierce, "Traveling-Wave Tubes," D. Van Nostrand Co., New York, N. Y., ch. 4; 1950.

Ridge waveguides are also used as H-type output transformers in magnetrons for the purpose of transforming the high impedance of the waveguide used for power transmission to the low impedance level of the magnetron. If a rectangular waveguide transformer is employed, the dimensions required for impedance matching may be too large, especially for magnetrons having short block heights. When the H-type transformer is used, an effectively large width can be obtained with small physical sizes. In addition, good broadband characteristics may be provided by proper selection of the dimensions of the H section to yield a cutoff wavelength at least as long as that of the waveguide connected to the transformers.

In these applications of ridge waveguides, the cutoff wavelength and the characteristic impedance are important parameters to be known for design purposes, and approximate relations for their determination have been available.[5-7] Cohn[8] first developed the accurate transcendental expressions for cutoff wavelengths of odd and even TE_{mo} modes and also expressions for the attenuation and characteristic impedance of the TE_{10} mode. Recently Cohn's work has been extended to include unusual ridge dimensions and cross sections other than rectangular.[8-10] In this article, emphasis is laid upon the calculation of the dominant mode characteristics of rectangular ridge waveguides. Formulas for finding these characteristics are expressed explicitly in terms of the guide dimensions, and charts are constructed to facilitate computations for waveguides having various aspect ratios and having ridges of different widths and depths.

Cutoff Wavelengths for the Dominant Mode in Ridge Waveguides

Cross sections of single-ridge and double-ridge waveguides are shown in Fig. 1. In the derivations, mks units are used unless otherwise mentioned. In Fig. 2, a unit length of ridge waveguide is represented by a lumped-constant equivalent circuit consisting of capacitance and inductance in parallel. The capacitance, C, in the equivalent circuit consists of the electrostatic capacitance, C_s, and the discontinuity capacitance, C_d. When a single-ridge waveguide such as that shown in Fig. 1(a) is operating in the dominant mode, the capacitance, C_s, depends mainly on the region between the ridge and

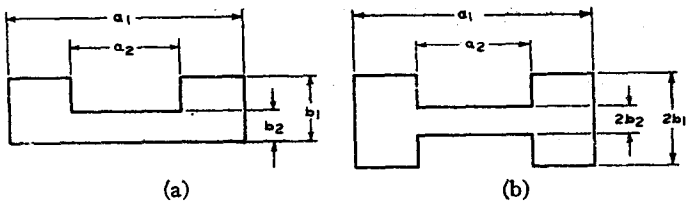

Fig. 1—Cross sectional view of (a) single-ridge and (b) double-ridge waveguides.

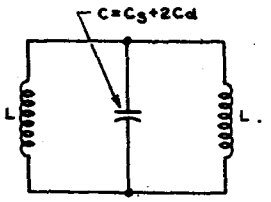

Fig. 2—Equivalent lumped-constant circuit for a unit length of ridge waveguide at cutoff wavelength.

the bottom plate, where a strong electric field exists This capacitance in farads per unit length of the guide is approximately given by

$$C_s = \frac{\epsilon a_2}{b_2} \tag{1}$$

where ϵ is the permittivity of the medium and in free-space equals 8.854×10^{-12} farad per meter.

The ridge in the waveguide presents discontinuities to the electromagnetic waves and causes local or higher-order waves. The effects of these local fields are included in the calculation by the addition at the proper location of the discontinuity susceptance which is here capacitive in nature. By the use of Hahn's method[11] of field matching, Whinnery and Jamieson[12] developed a series for the discontinuity capacitance, C_d, which depends on the step ratio, b_2/b_1, and, to a lesser extent, on the ratio a_2/b_2. The capacitance C_d along with the quantity $2C_d/\epsilon$ is plotted in Fig. 3 as a function of the step ratio b_2/b_1.

This discontinuity capacitance approaches closely the fringing capacitance in a constricted conductor, which is obtained by means of Schwarz-Christoffel transformation[12,13]

$$C_d = \frac{\epsilon}{\pi}\left[\frac{x^2+1}{x}\cosh^{-1}\left(\frac{1+x^2}{1-x^2}\right) - 2\ln\frac{4x}{1-x^2}\right] \tag{2}$$

where $x = b_2/b_1$. The value of C_d found from (2) can be shown to agree with that given by Fig. 3. The total capacitance C in farads per unit length of the waveguide is then

$$C = \frac{\epsilon a_2}{b_2} + 2C_d. \tag{3}$$

[5] G. B. Collins, ed., "Microwave Magnetrons," M.I.T. Rad. Lab. Ser., McGraw-Hill Book Co., Inc., New York, N. Y., vol. 6, pp. 198–203; 1948.
[6] G. L. Ragan, ed., "Microwave Transmission Circuits," M.I.T. Rad. Lab. Ser., McGraw-Hill Book Co., Inc., New York, N. Y., vol. 9, p. 57; 1948.
[7] S. Ramo and J. R. Whinnery, "Fields and Waves in Modern Radio," John Wiley and Sons, Inc., New York, N. Y.; 1944.
[8] Hans-Georg Unger, "Die Berechnung von Steghohlleitern," *Archiv Elekt. Uebertragung*, Band 9, Heft 4; April, 1955.
[9] J. M. Osepchuk, "Variational Calculations on Ridge Waveguides," Cruft Lab., Harvard Univ., Cambridge, Mass., Tech. Rep. No. 224; May 5, 1955.
[10] S. Hopfer, "The design of ridged waveguides," IRE Trans., vol. MTT-3, pp. 20–29; October, 1955.
[11] W. C. Hahn, "A new method for the calculation of cavity resonators," *J. Appl. Phys.*, vol. 12, pp. 62–68; January, 1941.
[12] J. R. Whinnery and H. W. Jamieson, "Equivalent circuits of discontinuities in transmission lines," Proc. IRE, vol. 32, pp. 98–116; February, 1944.
[13] Miles Walker, "Conjugate Functions for Engineers," Oxford University Press, Cambridge, Mass.; 1933.

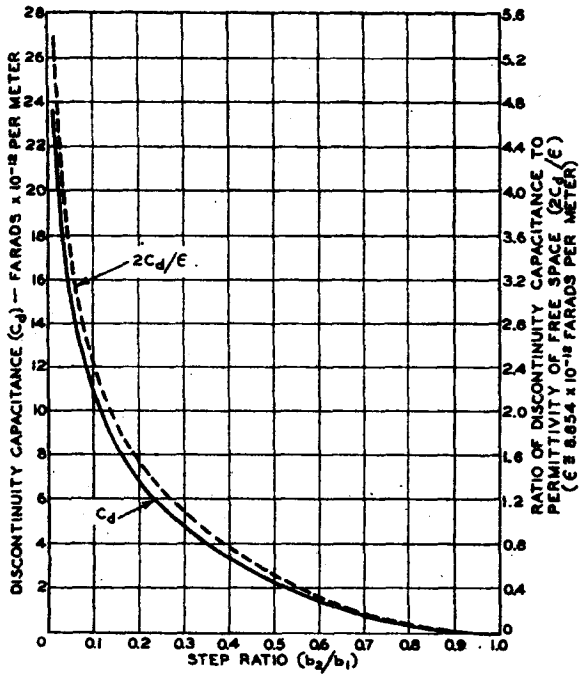

Fig. 3—Discontinuity capacitance, C_d, and the ratio, $2C_d/\epsilon$ as functions of the step ratio, b_2/b_1.

The inductances in the equivalent circuit show in Fig. 2 are determined by the sections of the waveguide on both sides of the ridge as shown in Fig. 1(a). The inductance, L, in henries due to either section per unit length of waveguide is given by

$$L = \frac{\mu(a_1 - a_2)}{2}(b_1), \tag{4}$$

where μ is the permittivity of the medium and equals $4\pi \times 10^{-7}$ henry per meter for free space. For the double-ridge waveguide depicted in Fig. 1(b), the capacitance C in (3) should be halved, and the inductance L in (4) doubled; the cutoff frequency remains unchanged.

At cutoff, the waves travel back and forth in the ridge waveguide in the transverse direction without longitudinal propagation; this condition corresponds to anti-resonance in the circuit shown in Fig. 2. The cutoff frequency, f_c', of the ridge waveguide in cycles per second is

$$f_c' = \frac{1}{2\pi\sqrt{(L/2)C}} \tag{5}$$

which, in conjunction with (3) and (4), becomes

$$f_c' = \frac{1}{\pi\sqrt{\mu\epsilon}\sqrt{\left(\frac{a_2}{b_2} + \frac{2C_d}{\epsilon}\right)(a_1 - a_2)(b_1)}}. \tag{6}$$

The cutoff wavelength, λ_c', of the ridge waveguide is given by $\lambda_c' = 1/(f_c'\sqrt{\mu\epsilon})$ and the cutoff wavelength λ_c of rectangular waveguide of width a_1 by $\lambda_c = 2a_1$. The ratio of these two cutoff wavelengths is

$$\frac{\lambda_c'}{\lambda_c} = \frac{\pi}{2}\sqrt{\left(\frac{a_2}{b_2} + \frac{2C_d}{\epsilon}\right)\left(\frac{b_1}{a_1}\right)\left(1 - \frac{a_2}{a_1}\right)}. \tag{7}$$

A nomograph for the determination of λ_c'/λ_c for ridge waveguides having known dimensions is shown in Fig. 4 (opposite). The value of $2C_d/\epsilon$ corresponding to a given step ratio, b_2/b_1, is found from Fig. 3. A line joining this value and the given point on the a_2/b_2 scales determines the sum $(a_2/b_2 + 2C_d/\epsilon)$. A second line is then drawn connecting the two given points a_1/b_1 and a_2/a_1 on the horizontal scales and cutting the diagonal at a definite point. A final line from the point $(a_2/b_2 + 2C_d/\epsilon)$ through this intersection determines the value of λ_c'/λ_c on the right-hand scale.

Cutoff Wavelengths for the Higher Modes in Ridge Waveguides

To find the cutoff wavelengths of higher modes, the single-ridge waveguide shown in Fig. 1(a) is considered as a composite transmission-line system having waves traveling in the transverse direction.[8] In Fig. 5(a), one half of a length, d, of the guide is represented by two sets of parallel plates separated by distances b_1 and b_2. The odd mode of the TE_{m0} wave requires a voltage loop and a current node at the center of the waveguide; the equivalent circuit shown in Fig. 5(b) should have an open circuit at the left end and a short circuit at the right end. In this circuit,

$\theta_1 = \left(1 - \frac{a_2}{a_1}\right)\frac{\lambda_c}{\lambda_c'}\frac{\pi}{2}$ = electrical length of section X_1 in radians.

$\theta_2 = \frac{a_2}{a_1}\frac{\lambda_c}{\lambda_c'}\frac{\pi}{2}$ = electrical length of section X_2 in radians.

$Y_{01} = \sqrt{\frac{\epsilon}{\mu}}\left(\frac{d}{b_1}\right)$ = characteristic admittance of section X_1 in mhos.

$Y_{02} = \sqrt{\frac{\epsilon}{\mu}}\left(\frac{d}{b_2}\right)$ = characteristic admittance of section X_2 in mhos.

$B_c' = 2\pi f_c' dC_d$ = discontinuity susceptance for a length d of the composite line in mhos.

The cutoff condition of the waveguide corresponds to resonance of the equivalent circuit,[8,10,14] which leads to an expression giving the cutoff wavelength, λ_c', implicitly in terms of the guide dimensions

$$\frac{b_1}{b_2} = \frac{\cot\left[\left(1 - \frac{a_2}{a_1}\right)\frac{\lambda_c}{\lambda_c'}\frac{\pi}{2}\right] - \frac{2C_d}{\epsilon}\frac{b_1}{a_1}\frac{\lambda_c}{\lambda_c'}\frac{\pi}{2}}{\tan\left(\frac{a_2}{a_1}\frac{\lambda_c}{\lambda_c'}\frac{\pi}{2}\right)}. \tag{8}$$

This equation is solved for the first order root to obtain the cutoff wavelength of the TE_{10} mode and for higher-

[14] N. Marcuvitz, "Waveguide Handbook," M.I.T. Rad. Lab. Ser., McGraw-Hill Book Co., Inc., New York, N. Y., vol. 10, pp. 399–402; 1951.

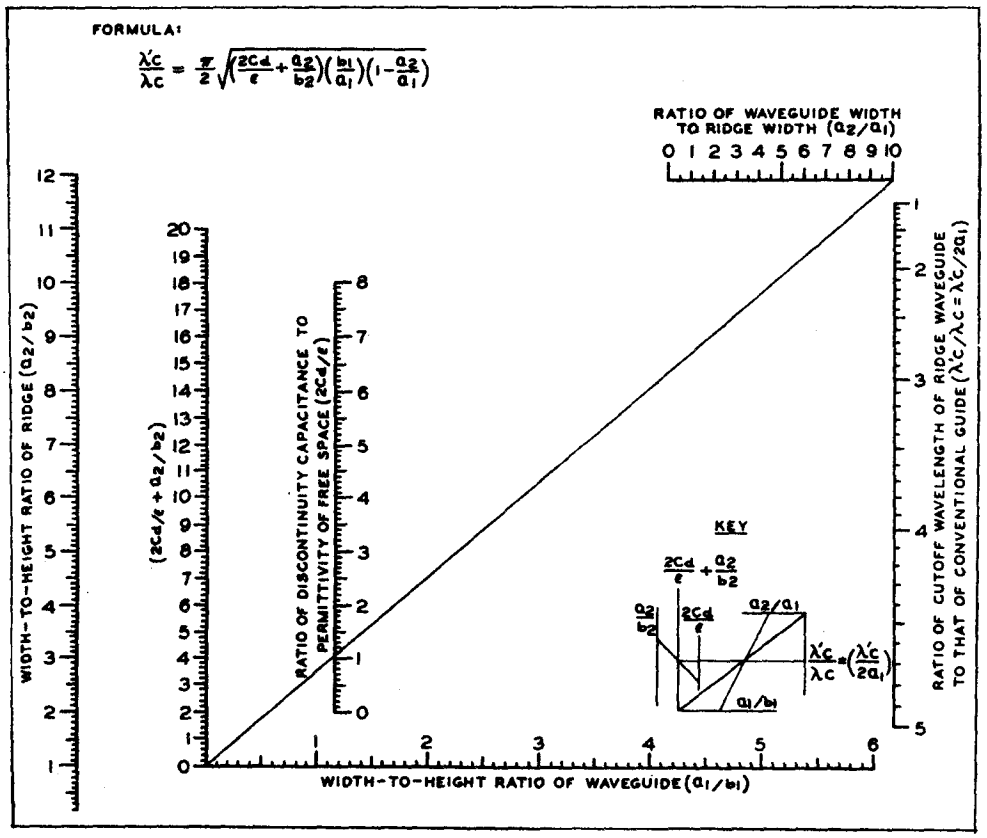

Fig. 4—Nomograph for the determination of the ratio, λ_c'/λ_c, of the cutoff wavelength, λ_c', of a ridge waveguide to the cutoff wavelength, λ_c, of a conventional rectangular waveguide having the same internal dimensions.

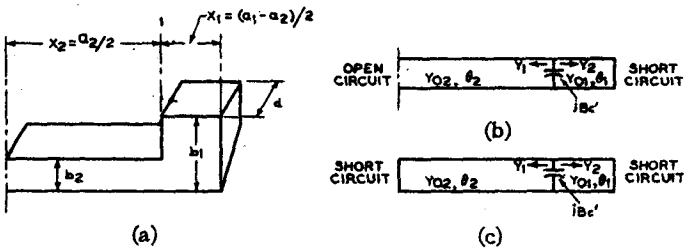

Fig. 5—Equivalent distributed parameter circuits for one half of a unit length of (a) ridge waveguide, (b) for odd modes of TE_{mo} waves, and (c) for even modes.

order roots to obtain the cutoff wavelengths of the higher-order odd TE_{mo} modes.

Because the ratios appearing in the arguments of the trigonometric functions are substantially less than unity, these functions can be replaced by the first two terms of their series expansions. Eq. (8) then becomes

$$\left[\frac{b_1}{b_2}\left(\theta_2+\frac{1}{3}\theta_2^3\right)+\frac{2C_d}{\epsilon}\frac{b_1}{a_2}\theta_2\right]\cdot\left[\left(\frac{a_1}{a_2}-1\right)\theta_2+\frac{1}{3}\left(\frac{a_1}{a_2}-1\right)^3\theta_2^3\right]=1. \quad (9)$$

When the cubic terms in (9) are discarded and remaining terms are solved for λ_c'/λ_c, (7) is obtained.

To improve the accuracy of λ_c'/λ_c determined from the chart, this approximate value is substituted only in the cubic terms of (9); the result is a quadratic equation θ_2 or in λ_c/λ_c'. This equation can be solved readily to obtain a more accurate value of λ_c'/λ_c.

The even modes of the TE_{mo} waves have voltage nodes at the center and at the end of the waveguide section in Fig. 5(a); the equivalent circuit for these modes becomes Fig. 5(c). The cutoff wavelengths of the TE_{20} and higher-order even modes as determined by the resonance of this circuit are given by

$$\frac{b_1}{b_2}=\frac{\frac{2C_d}{\epsilon}\frac{b_1}{a_1}\frac{\lambda_c}{\lambda_c'}\frac{\pi}{2}-\cot\left[\left(1-\frac{a_2}{a_1}\right)\frac{\lambda_c}{\lambda_c'}\frac{\pi}{2}\right]}{\cot\left(\frac{a_2}{a_1}\frac{\lambda_c}{\lambda_c'}\frac{\pi}{2}\right)}. \quad (10)$$

Characteristic Impedance of Ridge Waveguide

The characteristic impedance of ridge waveguide derived on the voltage-to-current basis is used in the calculation of tuning curves for a magnetron which is tuned by means of a ridge cavity attached to one of the magnetron resonators. This parameter is also used in impedance-matching problems. In the formulation of the voltage-to-current ratio, the current is separated into two components: 1) a longitudinal component on the top and bottom plates of the waveguide, which excites the principal fields, and 2) another longitudinal component at the point where the waveguide height changes, which produces the local fields.